The Journal of Chemical Physics

Forward–backward asymmetry in electron impact ionization of CO

Cite as: J. Chem. Phys. **152**, 164301 (2020); https://doi.org/10.1063/5.0006256
Submitted: 01 March 2020 . Accepted: 31 March 2020 . Published Online: 22 April 2020

Noboru Watanabe, and Masahiko Takahashi

The Journal of Chemical Physics ARTICLE scitation.org/journal/jcp

Forward–backward asymmetry in electron impact ionization of CO

Cite as: J. Chem. Phys. 152, 164301 (2020); doi: 10.1063/5.0006256
Submitted: 1 March 2020 • Accepted: 31 March 2020 •
Published Online: 22 April 2020

Noboru Watanabe[a] and Masahiko Takahashi

AFFILIATIONS

Institute of Multidisciplinary Research for Advanced Materials, Tohoku University, Sendai 980-8577, Japan

[a]Author to whom correspondence should be addressed: noboru.watanabe.e2@tohoku.ac.jp

ABSTRACT

We experimentally investigate the molecular-orientation dependence of high-energy electron-impact ionization of CO. The direction of the molecular-axis with respect to the momentum transfer vector $\boldsymbol{K}$ is deduced from the angular correlation between the fragment ion and the scattered electron. The experimental results on the $3\,^2\Pi$ ionization reveal that at small momentum transfer, the ionization probability near the threshold is higher when $\boldsymbol{K}$ points toward the C atom along the molecular axis than when it is in the opposite direction. Such a forward–backward asymmetry does not appear in single-photon ionization and requires non-dipole contributions. It is also shown that the $\{4\,^2\Sigma^+ + 5\,^2\Sigma^+ + 6\,^2\Sigma^+\}$ ionization preferentially takes place in the vicinity of the molecular orientation parallel to $\boldsymbol{K}$ at small momentum transfer, while non-dipole contributions cause the decrease in the relative intensity of the parallel direction.

I. INTRODUCTION

Photo- and electron-induced ionization of molecules has long been the subject of numerous studies due to its fundamental importance in various research fields such as molecular spectroscopy, astrophysics, and plasma physics.[1–3] Owing to the non-spherical symmetry of molecules, ionization probability varies with the orientation of the target molecule. The molecular-orientation dependence is well understood for ionization by single-photon absorption; the photoionization cross section is proportional to $\cos^2\chi$, with χ being the angle between the photon polarization vector and transition dipole moment of the molecule. By contrast, our knowledge about the molecular-orientation dependence of electron impact ionization is quite limited. Indeed, only a small number of experimental studies have been reported so far because of difficulties in measuring the electron scattering cross sections in the molecular frame.[4–10] An essential difference between the photo- and electron-induced processes is that the latter is not restricted by the dipole selection rule and electric quadrupole and higher multi-pole interactions contribute to the reaction. Non-dipole contributions are thus of key importance for understanding the electron-impact ionization dynamics.

Angle-resolved electron energy loss spectroscopy (AR-EELS) offers a good opportunity to investigate the non-dipole contributions.[11–14] AR-EELS is a high-energy electron scattering experiment in which the scattering cross section is measured as a function of energy and momentum transferred from the incident electron to the target. An excitation process of interest can be selected from the value of the electron energy loss, and its transition probability can be measured as a function of the momentum transfer. Of particular interest is that the influence of non-dipole interactions increases with the magnitude of the transferred momentum, while dipole interaction is dominant at the limit of zero momentum transfer. Thereby, AR-EELS allows us to investigate how ionization dynamics change from the dipole-regime caused by non-dipole contributions.

Although AR-EELS studies on molecules had long been restricted to investigating targets with random orientations, we have recently developed a method to perform EELS experiments in which the orientation of the molecular-axis is specified.[15–18] If the molecular ion formed by electron impact dissociates much faster than it rotates, the direction of the fragment ion departure coincides with the orientation of the target molecule. Hence, within the axial-recoil approximation,[5,19] the electron scattering cross section can be measured in the molecular frame by detecting not only the scattered electron but also the fragment ion. By using this (e, e+ion) technique, the molecular-orientation dependence of the inner valence ionization in N_2[16,17] and O_2[18] has been measured as a function of the

angle made between the momentum transfer vector and the molecular axis. The angular distributions thus obtained have shown clear momentum transfer dependence.

In this work, we have applied the (e, e+ion) technique to a heteronuclear diatomic molecule, CO. The main purpose of this study is to advance our understanding of stereodynamics in electron impact ionization of molecules. The molecular-orientation dependence of ionization probability is inherently affected by the shape of the target molecule and is inversion symmetric for a homonuclear diatomic molecule due to the $D_{\infty h}$ molecular symmetry. One may conceive that the inversion symmetry is broken in the ionization of a heteronuclear molecule. For instance, the ionization cross section of CO may be different depending upon whether the momentum transfer vector points toward the C or O atom. It should be noted, however, that such a forward–backward asymmetry does not appear in single-photon ionization if the ionized electron is not detected, since the molecular orientation dependence is described by a symmetric function $1 + \beta P_2(\cos\phi)$, where β is a constant and $P_2(\cos\phi)$ is the Legendre polynomial of the second order with ϕ being the angle between the photon polarization vector and the molecular axis.[20] The same is true for electron impact ionization at zero momentum transfer, where dipole interaction is dominant, and the appearance of the forward–backward asymmetry requires non-dipole contributions. To the best of our knowledge, despite the fundamental nature of molecular ionization in the non-dipole regime, however, the inversion asymmetry with respect to the direction of the momentum transfer vector has not been observed. To elucidate how the inversion asymmetry appears in electron impact ionization, we have examined the molecular-orientation dependence of the inner valence ionization of CO.

II. EXPERIMENT

The experimental procedures employed in this work are similar to those used in our previous (e, e+ion) studies,[16–18] and thus, only a brief description will be given here. An electron–ion coincidence apparatus used consists of an electron gun, an energy-dispersive electron spectrometer equipped with a deceleration lens system, and an ion momentum imaging spectrometer.[15] A continuum electron beam generated by the electron gun is chopped at 62.5 kHz by applying voltage pulses to a deflector electrode placed before exit apertures. The duty cycle of the electron gun is 1.0%. The pulsed electron beam is crossed with the molecular beam effusing from a gas nozzle with 0.5 mm inner diameter. Electrons scattered at a particular angle of θ with respect to the incident electron beam are decelerated to ~53 eV by means of the lens system and dispersed by a hemi-spherical analyzer. The electrons are then detected by a microchannel plate detector with a delay line anode for position readout. Upon the detection of an electron, a pulsed electric field is applied to the interaction region to extract ions into the momentum imaging spectrometer, equipped with a time- and position-sensitive detector. The recoil-momentum of an ion can be determined from its time of flight and arrival positions at the detector. The background due to false coincidences has been inferred by measuring ions produced by the incident electron pulse that passes through the interaction region shortly after the detection of an electron. The ions collected in this way are uncorrelated to the detected electron and thus provide the contribution of false coincidence events.

Electron–ion coincidence experiments were carried out for CO at scattering angles of $\theta = 2.2°$, 4.2°, and 8.2°. The CO gas used was purchased from Taiyo Nippon Sanso Co. It has a minimum stated purity of 99.95%. Electron impact energies of 1393 eV, 1398 eV, 1403 eV, 1408 eV, and 1413 eV were used in the measurements to cover a wider energy loss region. The spectra obtained at different impact energies were normalized in the overlapping E regions and combined with each other. The uncertainties of each scaling factor used in the normalization procedure have been inferred to be 1–4% for $\theta = 8.2°$ and 1–2% for $\theta = 2.2°$ and 4.2°. The instrumental energy resolution for electrons was estimated to be 0.8 eV full width at half maximum from the peak profile of the elastic scattering. The C^+ and O^+ fragment ions can be distinguished from each other by their flight times. Details of the estimation of the ion momentum resolution were described in our previous paper.[15] The experimental result was obtained by accumulating data at an ambient sample gas pressure of 1.0×10^{-4} Pa for 1–4 weeks runtime at each incident electron energy and scattering angle.

III. THEORY

In our earlier work,[17] an analytical form of the molecular-orientation dependence was derived for high-energy electron impact ionization. Briefly, within the Born approximation, the electron scattering cross section is proportional to the differential generalized oscillator strength (GOS), df/dE,[11,12]

$$\frac{df(\boldsymbol{K},E)}{dE} = \frac{2E}{K^2}\sum_n |T_{n0}|^2 \delta(E - E_{n0}). \tag{1}$$

Here, T_{n0} denotes the transition matrix element,

$$T_{n0} = \langle \Phi_n | \sum_j \exp(i\boldsymbol{K}\cdot\boldsymbol{r}_j) | \Phi_0 \rangle, \tag{2}$$

where Φ_0 and Φ_n are the wavefunctions of the initial and final target states, respectively, E_{n0} is the energy difference between these states, and $\boldsymbol{r}_j$ is the coordinate of the jth electron. Linear momentum transferred from the incident electron to the target is denoted as $\boldsymbol{K}$. What is observed in conventional AR-EELS experiments is that the GOS is averaged over the direction of the momentum transfer, $(4\pi)^{-1} \int df(\boldsymbol{K},E)/dE\, \Omega_{\boldsymbol{K}}$,[12–14] while the ($e$, e+ion) technique makes it possible to measure the dependence on the $\boldsymbol{K}$ orientation relative to the molecular axis. The magnitude of $\boldsymbol{K}$ is related to the scattering angle θ as $K = \{|\boldsymbol{k}_0|^2 + |\boldsymbol{k}_1|^2 - 2|\boldsymbol{k}_0||\boldsymbol{k}_1|\cos\theta\}^{1/2}$, where $\boldsymbol{k}_0$ and $\boldsymbol{k}_1$ are the momenta of the incident and scattered electrons. It may be worthwhile to note that when $K \sim 0$, the exponential term in Eq. (2) can be approximated as $\exp(i\boldsymbol{K}\cdot\boldsymbol{r}_j) = 1 + i\boldsymbol{K}\cdot\boldsymbol{r}_j$ and T_{n0} is proportional to the dipole transition matrix element,[11,12]

$$\lim_{K\to 0} T_{n0} = iK\langle \Phi_n | \sum_j \widehat{\boldsymbol{K}}\cdot\boldsymbol{r}_j | \Phi_0 \rangle$$

with $\widehat{\boldsymbol{K}} = \boldsymbol{K}/|\boldsymbol{K}|$, which plays an equivalent role as the polarization vector of light in photoabsorption.

For electron-impact ionization, the transition matrix can be written as

$$T_{n0} = \left\langle \psi_{\boldsymbol{p}}^{(-)} \Phi_n^{ion} \middle| \sum_j \exp(i\boldsymbol{K}\cdot\boldsymbol{r}_j) \middle| \Phi_0 \right\rangle = \left\langle \psi_{\boldsymbol{p}}^{(-)}(\boldsymbol{r}) \middle| \exp(i\boldsymbol{K}\cdot\boldsymbol{r}) \middle| \varphi_n(\boldsymbol{r}) \right\rangle, \tag{3}$$

where $\psi_{\boldsymbol{p}}^{(-)}$ is the wavefunction of the ejected electron having momentum $\boldsymbol{p}$ and φ_n is the Dyson orbital, defined as the overlap between the N-electron neutral state Φ_0 and the $(N-1)$-electron ionic state Φ_n^{ion}. Here, we expand $\psi_{\boldsymbol{p}}^{(-)}$ in terms of spherical harmonics as

$$\psi_{\boldsymbol{p}}^{(-)} = \sum_{l_{ej},m_{ej}} i^{l_{ej}} e^{-i\delta_{l_{ej},m_{ej}}} Y^*_{l_{ej}m_{ej}}(\widehat{\boldsymbol{p}}) R_{p,l_{ej},m_{ej}}(\boldsymbol{r}), \tag{4}$$

where $\delta_{l_{ej},m_{ej}}$ is the phase shift of a partial wave with the azimuthal quantum number l_{ej} and the magnetic quantum number m_{ej}. Similarly, the exponential term is expanded as

$$\exp(i\boldsymbol{K}\cdot\boldsymbol{r}) = 4\pi \sum_{l,m_\gamma} i^l j_l(Kr) \sqrt{\frac{2l+1}{4\pi}} Y_{lm_\gamma}(\widehat{\boldsymbol{r}}) D^l_{m_\gamma 0}(\widehat{\boldsymbol{R}}_\gamma), \tag{5}$$

where $j_l(Kr)$ denotes the spherical Bessel function of order l and $D^l_{m_\gamma 0}(\widehat{\boldsymbol{R}}_\gamma)$ is the Wigner rotation matrix[21] with $\widehat{\boldsymbol{R}}_\gamma$ being the Euler angle specifying the orientation of the molecule. The Euler angle is defined with respect to the laboratory-frame coordinate system in which the z-axis is chosen parallel to the direction of $\boldsymbol{K}$. Substitution of Eqs. (4) and (5) into Eq. (3) yields the following expression:

$$T_{n0} = \sum_{l,l_{ej},m_{ej},m_\gamma} i^{l-l_{ej}} e^{i\delta_{l_{ej},m_{ej}}} Y_{l_{ej}m_{ej}}(\widehat{\boldsymbol{p}}) D^l_{m_\gamma 0}(\widehat{\boldsymbol{R}}_\gamma) d_{l_{ej},m_{ej},l,m_\gamma}(K), \tag{6}$$

where

$$d_{l_{ej},m_{ej},l,m_\gamma}(K) = \sqrt{4\pi(2l+1)} \langle R_{p,l_{ej},m_{ej}} | j_l(Kr) Y_{lm_\gamma}(\widehat{\boldsymbol{r}}) | \varphi_n \rangle. \tag{7}$$

Since the angular momentum around the molecular axis is conserved for a linear molecule, m_{ej} is equal to $m_\gamma + m_n$, where m_n is the angular momentum quantum-number of the Dyson orbital.

In $(e, e+\text{ion})$ measurements, the ejected electron is not detected, and hence, its emission angle cannot be determined. We therefore integrate $|T_{n0}|^2$ over the solid angle of the electron emission and further take the summation over m_n to take into account the degeneracy of the final ionic state. As a consequence, the following expression is obtained:

$$\sum_{m_n} \int |T_{n0}|^2 d\widehat{\boldsymbol{p}} = \sum_{L_\gamma=0} b_{L_\gamma} D^{L_\gamma}_{00}(\widehat{\boldsymbol{R}}_\gamma), \tag{8}$$

where

$$b_{L_\gamma} = \sum_{l,l'} \langle l0, l'0 | L_\gamma 0 \rangle \sum_{l_{ej},m_{ej},m_n} i^{l-l'} d_{l_{ej},m_{ej},l,m_{ej}-m_n} d^*_{l_{ej},m_{ej},l',m_{ej}-m_n} \times (-1)^{m_n - m_{ej}} \langle l m_{ej} - m_n,\ l' - m_{ej} + m_n | L_\gamma 0 \rangle. \tag{9}$$

For a linear molecule, the Wigner rotation matrix $D^{L_\gamma}_{00}(\widehat{\boldsymbol{R}}_\gamma)$ can be replaced with the Legendre polynomial of order L_γ, $P_{L_\gamma}(\cos\phi_{\boldsymbol{K}})$. Here, $\phi_{\boldsymbol{K}}$ is the angle of the molecular axis with respect to $\boldsymbol{K}$. Thereby, the ion angular distribution $I(\phi_{\boldsymbol{K}})$ can be written as

$$I(\phi_{\boldsymbol{K}}) = C\left\{1 + \sum_{i=1} \beta_i P_i(\cos\phi_{\boldsymbol{K}})\right\}, \tag{10}$$

where C is a proportional constant and $\beta_i = b_i/b_0$. It should be noted that $P_i(z) = P_i(-z)$ when i is an even number, while $P_i(z) = -P_i(-z)$ in case i is an odd number. For a homonuclear diatomic molecule, the terms with an odd number of i vanish due to the $D_{\infty h}$ molecular symmetry, and as a consequence, $I(\pi + \phi_{\boldsymbol{K}})$ coincides with $I(\phi_{\boldsymbol{K}})$. Owing to the cylindrical symmetry of the linear molecule, $I(\pi + \phi_{\boldsymbol{K}}) = I(\pi - \phi_{\boldsymbol{K}})$, and thus, the angular distribution is symmetric about $\phi_{\boldsymbol{K}} = 90°$: $I(\phi_{\boldsymbol{K}}) = I(\pi - \phi_{\boldsymbol{K}})$. On the other hand, the terms with an odd number of i may contribute to the angular distribution of a heteronuclear diatomic molecule, and asymmetric ion emission, $I(\phi_{\boldsymbol{K}}) \neq I(\pi - \phi_{\boldsymbol{K}})$, can possibly arise. As discussed in our earlier paper,[17] if K is not significantly large, the magnitude of b_i with large i is negligibly small, and hence, the terms with $i \geq 5$ are omitted from Eq. (10) in the data analysis described later.

When $K = 0$, the GOS coincides with the optical oscillator strength (OOS) and $I(\phi_{\boldsymbol{K}})$ becomes equivalent to the photoion angular distribution, $I_p(\phi)$. Here, ϕ indicates the angle of the molecular axis with respect to the photon polarization vector. $I_p(\phi)$ is proportional to $\{1+ \beta P_2(\cos\phi)\}$ and characterized by the asymmetry parameter β.[20] It follows that

$$\beta_2(K)|_{K=0} = \beta, \tag{11a}$$

$$\beta_i(K)|_{K=0} = 0 \quad (i \neq 2). \tag{11b}$$

Hence, $I(\phi_{\boldsymbol{K}})$ can be regarded as an extension of photoion angular distribution into the non-dipole regime. It should be noted that $I_p(\phi)$ is equal to $I_p(\pi + \phi)$ and thus inversion symmetric even for heteronuclear molecules.

IV. RESULTS AND DISCUSSION

The CO molecule belongs to the $C_{\infty h}$ point group, and its ground state has an electronic configuration of $(\text{core})^4(3\sigma)^2(4\sigma)^2(1\pi)^4(5\sigma)^2$.[22] Various dissociative ionic states may arise in the energy loss (E) region measured. The relevant ionization potentials (IP's) and their assignments[23–27] are listed in Table I. The cationic states in the energy region are primarily two-hole one-particle states.

Figure 1 presents the two-dimensional plots of energy correlation between the scattered projectile and fragment ions for $\theta = 2.2°$, which were constructed by plotting the number of electron-fragment ion coincidence events as a function of E and kinetic energy (KE) of the ion. Also presented in Fig. 1 are the fragment ion yield spectra for $\theta = 2.2°$, $4.2°$, and $8.2°$, which correspond to $K^2 = 0.16$ a.u., 0.56 a.u., and 2.10 a.u., respectively. The O^+ yield spectra for $\theta = 4.2°$ measured at different impact energies are inserted in

TABLE I. Vertical ionization potentials (IP's) of CO.

States	Vertical IP's (eV) Expt.	Theory[a]	Main configurations[25–27]
$D^2\Pi$	22.7[b]	23.65	$(5\sigma)^{-2}(2\pi)^{+1}$
$3\,^2\Sigma^+$	23.7[c]	24.53	$(1\pi)^{-1}(5\sigma)^{-1}(2\pi)^{+1}$
$3\,^2\Pi$	27.5[d]	28.31	$(4\sigma)^{-1}(5\sigma)^{-1}(2\pi)^{+1}$
$4\,^2\Sigma^+$	31.1[c]	30.16	$(1\pi)^{-1}(5\sigma)^{-1}(2\pi)^{+1}$
$5\,^2\Sigma^+$	32.0[c]	32.58	$(4\sigma)^{-1}(1\pi)^{-1}(2\pi)^{+1}$
$6\,^2\Sigma^+$		32.74	$(4\sigma)^{-1}(1\pi)^{-1}(2\pi)^{+1}$

[a]Symmetry adapted cluster-configuration interaction (SAC-CI) calculation.[26]
[b]Reference 23.
[c]Reference 24.
[d]Reference 25.

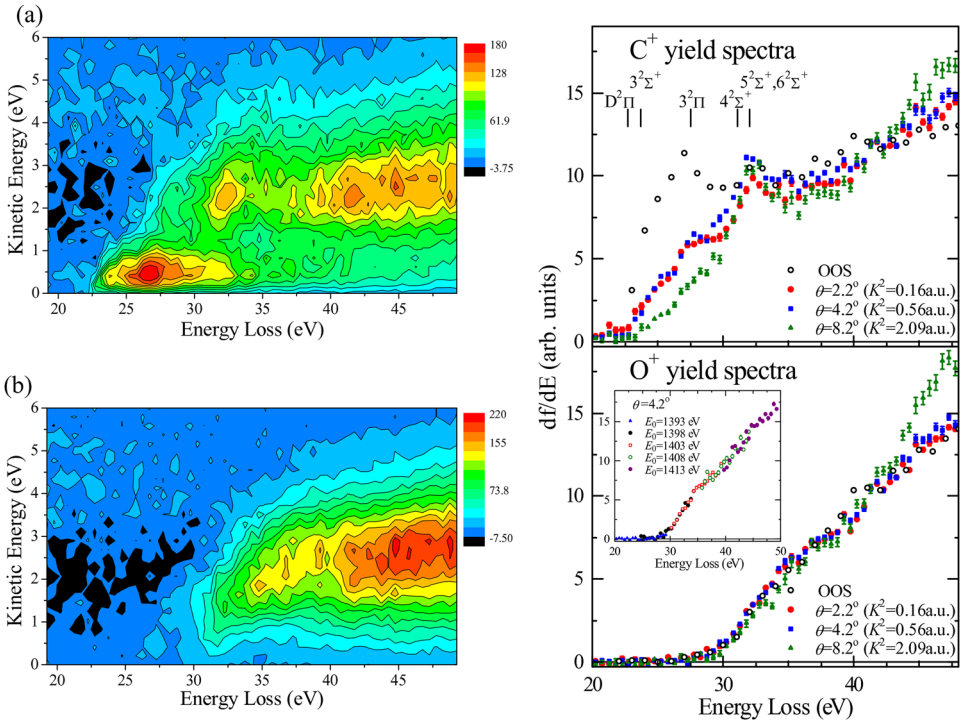

FIG. 1. (Left panels) Two-dimensional plots of energy correlation between the scattered electron and fragment ions for θ = 2.2°, which were obtained by plotting the number of (a) electron–C^+ and (b) electron–O^+ coincidence events as a function of electron energy loss and kinetic energy of the ion. (Right panel) Fragment-ion-yield spectra of CO constructed from the electron–ion coincident data for θ = 2.2°, 4.2°, and 8.2°. Open circles represent the associated optical oscillator strength (OOS) distributions,[28] which correspond to the results at zero momentum transfer. The inset in the right panel is the O^+ yield spectra for θ = 4.2° measured at different impact energies.

Fig. 1 to illustrate the level of consistency between the results. Vertical bars indicate IPs reported in the literature.[23–26] The spectra were obtained by projecting the E–KE correlation plots onto the energy loss axis and converting the results to relative GOS distributions by means of the Bethe–Born formula.[11,12] Errors bars shown are statistical only, though additional small uncertainties were introduced by the normalization procedure used to combine the spectra measured at different impact energies, as mentioned in Sec. II. Also depicted in Fig. 1 is the associated OOS distribution reported by Wight *et al.*,[28] which is equivalent to the GOS distribution at K^2 = 0. All spectra were normalized at E = 41 eV for ease of comparison of the spectral shapes.

In this work, we focus our attention on ionization to the 3 $^2\Pi$, 4 $^2\Sigma^+$, 5 $^2\Sigma^+$, and 6 $^2\Sigma^+$ states. As can be seen from Fig. 2, these cationic states are all directly dissociative, and the molecular orientation can be determined from the recoil direction of the fragment ion. On the other hand, the lower-lying cationic states, D $^2\Pi$ and 3 $^2\Sigma^+$, are both predissociative, and the axial recoil approximation would not be valid. These two CO^+ states can dissociate only into C^+ + O, and the KE of the C^+ ion is less than ~1 eV.[29–31] Thereby, the influences of the predissociative channels can be excluded by choosing coincidence events in which C^+ with KE > 1 eV or O^+ is detected.

First, we discuss the molecular-orientation dependence of the 3 $^2\Pi$ ionization. Photoelectron–photoion coincidence (PEPICO) studies[25,29] have revealed that one of the major dissociation pathways of the $3^2\Pi$ state is decay into the second lowest limit, $C^+(^2P)$ + $O(^1D)$. From the IP of ~27.5 eV[25,32] and the energy of the dissociation limit, 24.32 eV,[32] the KE of C^+ is deduced to be ~1.82 eV. It should be noted that C^+ ions with similar KE are generated also from the 4 $^2\Sigma^+$, 5 $^2\Sigma^+$, and 6 $^2\Sigma^+$ states. However, ionization to these states has a negligible influence on the coincidence data below E = 30 eV due to the higher IPs of > ~31 eV, and thus, the 3 $^2\Pi$ ionization near the threshold can be extracted from the analysis of C^+ KE.

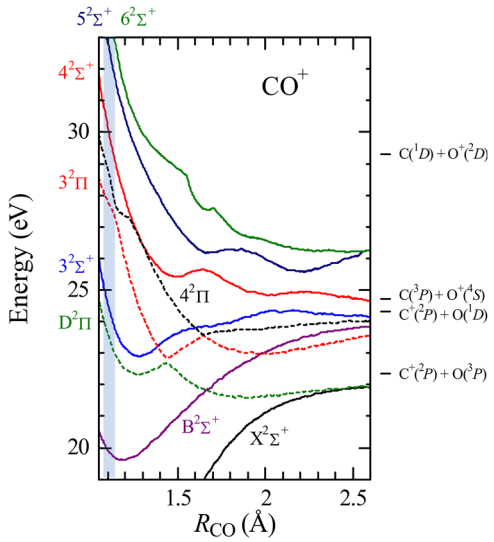

FIG. 2. Potential energy curves of the electronic states of CO^+ reported by Lebech *et al.*[25] The Franck–Condon region is indicated by the shaded region.

Keeping the above discussion in mind, we constructed the angular distributions of C^+ ions with KE = 1.8–2.3 eV for E = 28–30 eV to examine the molecular-orientation dependence of the 3 $^2\Pi$ ionization. The results are presented in Fig. 3 as a function of angle between the recoil direction of C^+ and the momentum transfer vector $\boldsymbol{K}$, ϕ_K. An analytic function described in Sec. III, $C\{1 + \sum_{i=1}^{4} \beta_i P_i(\cos\phi_K)\}$, was used to reproduce the experimental results, treating C and β_i's as fitting parameters. The fitted curves are shown as solid lines in Fig. 3. For ease of comparison, all data are scaled so that the proportional coefficient C becomes equal to 1. Also shown in Fig. 3 is the associated photoion angular distribution, $1 + \beta P_2(\cos\phi)$, with $\beta = 0.4$ reported by Lebech *et al.*[29]

It is evident from Fig. 3 that the 3$^2\Pi$ ionization exhibits anisotropic molecular-orientation dependence. For $K^2 = 0.16$ a.u., the angular distribution has a maximum around $\phi_K = 0°$, and its intensity is considerably higher than that at $\phi_K = 180°$, indicating that the 3 $^2\Pi$ ionization near the threshold preferentially occurs when the momentum transfer vector points toward the C atom. A similar tendency has been observed also for $K^2 = 0.56$ a.u. As was mentioned, such a forward–backward asymmetry of fragment ion emission does not arise in photoionization. Indeed, the photoion angular distribution shown in Fig. 3 is symmetric about 90°, and there is a significant difference between the photo- and electron-impact results. It is in contrast to our previous (e, e+ion) studies for N_2 and O_2.[17,18] At $K^2 = 0.16$ a.u., the inner valence ionization of these homonuclear molecules has shown molecular-orientation dependence similar to the associated photoion angular distributions, suggesting major contributions of dipole interaction in the ionization processes studied. The forward–backward asymmetry indicates that non-dipole contributions play a crucial role in the stereodynamics of the 3 $^2\Pi$ ionization even at the rather small K^2. With the increase in K^2 to 2.09 a.u., the molecular-orientation dependence is changed due to a larger influence of non-dipole interaction. The angular distribution for $K^2 = 2.09$ a.u. appears to be almost symmetric about 90°, though the large statistical error prevents us from making a detailed discussion.

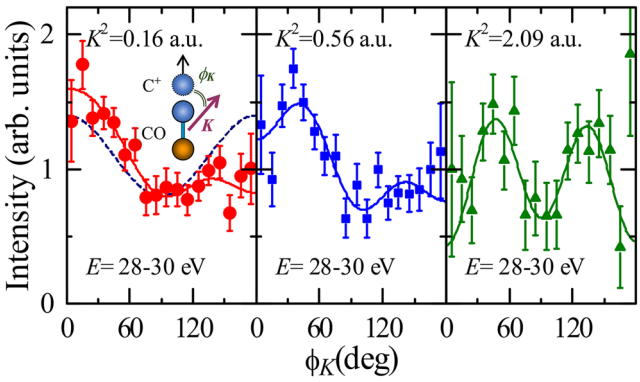

FIG. 3. Angular distributions of C^+ ions having KE = 1.8–2.3 eV for E = 28–30 eV, which are dominantly attributed to dissociation from the 3 $^2\Pi$ cationic state to $C^+(^2P)$ + $O(^1D)$. Solid lines represent the analytical function fitted to the experiment, $C\{1 + \sum_{i=1}^{4} \beta_i P_i(\cos\phi_K)\}$, and the dashed line is the associated photoion angular distribution, $1 + \beta P_2(\cos\phi)$, with $\beta = 0.4$ reported by Lebech *et al.*[29] For comparison in shape, all results are scaled so that the proportional coefficient C is equal to 1. See the text for details.

We subsequently investigate the molecular-orientation dependence of the ionization to the 4 $^2\Sigma^+$, 5 $^2\Sigma^+$, and 6 $^2\Sigma^+$ states. These are the first three cationic states from which O^+ is substantially generated. Thereby, for studying ionization to these states, electron–O^+ coincidence data are more suitable than electron–C^+ data because no contribution from the lower ionization channels is included in the former data. Since the IPs for further higher-lying states are larger than ~34 eV,[22,26] the electron–O^+ coincidence events at E = 30–34 eV come dominantly from the 4 $^2\Sigma^+$, 5 $^2\Sigma^+$, and 6 $^2\Sigma^+$ ionization, though contributions of the individual channels cannot be separated from one another due to similar KE distributions of O^+ ions generated from these cationic states.

In Fig. 4, we show the angular distributions of the O^+ ions for E = 30–32 eV and 32–34 eV, which were constructed from the electron–O^+ coincidence events in which O^+ having KE = 0.8–1.7 eV was detected. The O^+ ions would arise mainly from the dissociation of the 4 $^2\Sigma^+$, 5 $^2\Sigma^+$, and 6 $^2\Sigma^+$ states into the $C(^1D)$ + $O^+(^2D)$ limit.[25,29] For the convenience of comparison with the 3 $^2\Pi$ results, the angle between the momentum transfer vector and the molecular axis, ϕ_K, is defined so that 0° means $\boldsymbol{K}$ pointing from the O atom to the C atom. The associated photoion angular distribution is also depicted in Fig. 4 as dashed lines, assuming the β value of 1.1, measured by Lebech *et al.* at a photon energy of $h\nu$ = 32 eV.[29]

It can be seen from Fig. 4 that the angular distributions for $K^2 = 0.16$ a.u. exhibit a deep minimum at $\phi_K \sim 90°$ and have maxima around 0° and 180°, indicating that the ionization process preferentially takes place in the vicinity of the molecular orientation parallel to $\boldsymbol{K}$. Also seen from Fig. 4 is that the shape of the angular

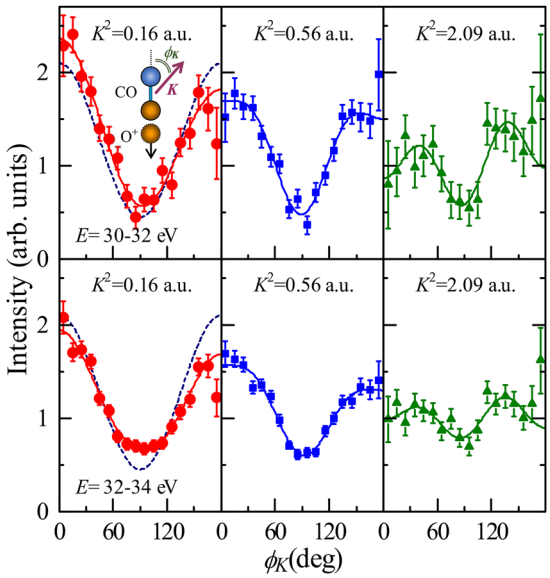

FIG. 4. Angular distributions of O^+ ions having KE = 0.8–1.7 eV, which are dominantly associated with the {4 $^2\Sigma^+$ + 5 $^2\Sigma^+$ + 6 $^2\Sigma^+$} ionization channel. For the convenience of comparison with the 3 $^2\Pi$ results, the angle ϕ_K is defined so that 0° means $\boldsymbol{K}$ pointing to the C atom. Solid lines represent the analytical function fitted to experiment, $C\{1 + \sum_{i=1}^{4} \beta_i P_i(\cos\phi_K)\}$, and dashed lines are the associated photoion angular distribution. All results are scaled so that the proportional coefficient C is equal to 1. See the text for details.

distributions for K^2 = 0.16 a.u. resembles the shape of the photoion angular distribution (dashed line). Despite the resemblance in shape, however, the electron impact results appear to be asymmetric about ϕ_K = 90° and have a slightly higher intensity at around 0° than at 180°. It strongly suggests that although the dipole interaction plays a major role in the ionization process studied, non-dipole contributions are not negligible even at the rather small K^2, 0.16 a.u. A comparison between the results at different K^2 shows that the relative intensities at $\phi_K \sim 0°$ and 180° decrease with the increase in K^2 and the difference from the photoion angular distribution becomes larger. In particular, the angular distributions for K^2 = 2.09 a.u. have maxima around ϕ_K = 45° and 135°. A similar tendency has been observed also for the inner valence ionization of N_2 and O_2,[17,18] and the maxima observed for K^2 = 2.09 a.u. may be attributed mainly to the contribution of the $\beta_4 P_4(\cos\phi_K)$ term in Eq. (10).

The forward–backward asymmetry of the fragment ion emission requires asymmetric shapes of the wavefunctions in the initial and/or final target states. Indeed, such an asymmetry has not been observed in the angular distributions for N_2 and O_2, having inversion symmetry.[17,18] It should be noted, however, that the molecular-orientation dependence of electronic excitation in heteronuclear molecules is not always asymmetric about ϕ_K = 90°. To account for this, we consider a transition between bound states of CO. The GOS of a discrete transition, $f(\boldsymbol{K})$, is proportional to the absolute square of the transition matrix element: $f(\boldsymbol{K}) \propto |T_{n0}|^2$. For a discrete transition, the wavefunctions of the initial and final target states, Φ_0 and Φ_n, can be taken as real-valued without loss of generality, and hence, the following relation holds:

$$|T_{n0}|^2 = \left|\langle\Phi_n|\sum_j \exp(i\boldsymbol{K}\cdot\boldsymbol{r}_j)|\Phi_0\rangle\right|^2 = \left|\langle\Phi_n|\sum_j \exp(-i\boldsymbol{K}\cdot\boldsymbol{r}_j)|\Phi_0\rangle\right|^2. \quad (12)$$

It indicates that $f(\boldsymbol{K})$ is equal to $f(-\boldsymbol{K})$. Thereby, the molecular-orientation dependence of the GOS is required to be inversion symmetric for a discrete transition even in a heteronuclear molecule.

This is not the case for direct ionization of CO because of the following reason. The wavefunction of the ejected electron behaves as an outgoing Coulomb wave at a point infinitely far from the residual molecular ion[33] and must be complex-valued to satisfy this boundary condition. Equation (12) does not hold for the complex valued wavefunction, and hence, the forward–backward asymmetry may arise in high-energy electron-impact ionization of CO. This consideration indicates that the outgoing-wave boundary condition essentially plays an important role in the stereodynamics of molecular ionization.

V. SUMMARY

In this work, we performed (e, e+ion) experiments on inner valence ionization of CO using an incident electron energy of 1.4 keV at K^2 = 0.16 a.u., 0.56 a.u., and 2.10 a.u. The angle of the molecular axis with respect to the momentum transfer vector was determined from the direction of the fragment ion departure. It has been shown that forward–backward asymmetry appears in the $3\,^2\Pi$ ionization for K^2 = 0.16 a.u. and 0.56 a.u., indicating that non-dipole contributions play a crucial role in the ionization process studied even at the rather small K^2. The angular distributions of O^+ ions have revealed that the $\{4\,^2\Sigma^+ + 5\,^2\Sigma^+ + 6\,^2\Sigma^+\}$ ionization near the threshold dominantly occurs in the vicinity of the molecular orientation parallel to $\boldsymbol{K}$ at small momentum transfer, while the relative intensity of the parallel direction decreases with the increase in K^2 due to non-dipole contributions.

This work provides an example of nontrivial molecular orientation effects evoked in the non-dipole regime. The present results offer a challenge to electron scattering theory since the influences of anisotropic molecular potential and the outgoing-wave boundary condition have to be correctly taken into account for describing the observed forward–backward asymmetry and its momentum transfer dependence. Furthermore, knowledge on the molecular orientation dependence gives a basis for the application of molecular-frame electron impact ionization to molecular spectroscopy, which may be used, for example, to extract information on the spatial shape of molecular orbitals.[5,10,18]

ACKNOWLEDGMENTS

This research was supported by the JSPS KAKENHI (Grant Nos. 18H01932 and 19K21862). It was also supported, in part, by the Management Expenses Grants for National Universities Corporation and the Cooperative Research Program of "NJRC Mater. & Dev."

The data that support the findings of this study are available from the corresponding author upon reasonable request.

REFERENCES

[1] J. W. McConkey, C. P. Malone, P. V. Johnson, C. Winstead, V. McKoy, and I. Kanik, Phys. Rep. **466**, 1 (2008), and references therein.
[2] O. Dutuit, N. Carrasco, R. Thissen, V. Vuitton, C. Alcaraz, P. Pernot, N. Balucani, P. Casavecchia, A. Canosa, S. L. Picard, J.-C. Loison, Z. Herman, J. Zabka, D. Ascenzi, P. Tosi, P. Franceschi, S. D. Price, and P. Lavvas, Astrophys. J., Suppl. Ser. **204**, 20 (2013).
[3] N. J. Mason, J. Phys. D: Appl. Phys. **42**, 194003 (2009), and references therein.
[4] M. Takahashi, N. Watanabe, Y. Khajuria, K. Nakayama, Y. Udagawa, and J. H. D. Eland, J. Electron Spectrosc. Relat. Phenom. **141**, 83 (2004).
[5] M. Takahashi, N. Watanabe, Y. Khajuria, Y. Udagawa, and J. H. D. Eland, Phys. Rev. Lett. **94**, 213202 (2005).
[6] S. Bellm, J. Lower, E. Weigold, and D. W. Mueller, Phys. Rev. Lett. **104**, 023202 (2010).
[7] A. Senftleben, T. Pflüger, X. Ren, O. Al-Hagan, B. Najjari, D. Madison, A. Dorn, and J. Ullrich, J. Phys. B: At., Mol. Opt. Phys. **43**, 081002 (2010).
[8] X. Ren, T. Pflüger, S. Xu, J. Colgan, M. S. Pindzola, A. Senftleben, J. Ullrich, and A. Dorn, Phys. Rev. Lett. **109**, 123202 (2012).
[9] J. C. A. Lower, E. Ali, S. Bellm, E. Weigold, A. Harris, C. G. Ning, and D. Madison, Phys. Rev. A **88**, 062705 (2013).
[10] D. B. Jones, M. Yamazaki, N. Watanabe, and M. Takahashi, Phys. Rev. A **87**, 022714 (2013).
[11] M. Inokuti, Rev. Mod. Phys. **43**, 297 (1971).
[12] K. T. Leung, J. Electron Spectrosc. Relat. Phenom. **100**, 237 (1999).
[13] A. P. Hitchcock, J. Electron Spectrosc. Relat. Phenom. **112**, 9 (2000).
[14] N. Watanabe, T. Hirayama, D. Suzuki, and M. Takahashi, J. Chem. Phys. **138**, 184311 (2013).
[15] N. Watanabe, T. Hirayama, S. Yamada, and M. Takahashi, Rev. Sci. Instrum. **89**, 043105 (2018).
[16] N. Watanabe, S. Yamada, and M. Takahashi, Phys. Rev. A **95**, 060702(R) (2017).
[17] N. Watanabe, S. Yamada, and M. Takahashi, Phys. Chem. Chem. Phys. **20**, 1063 (2018).

[18]N. Watanabe, S. Yamada, and M. Takahashi, Phys. Rev. A **99**, 022704 (2019).
[19]R. N. Zare, J. Chem. Phys. **47**, 204 (1967).
[20]S. Wallace and D. Dill, Phys. Rev. B **17**, 1692 (1978).
[21]M. E. Rose, *Elementary Theory of Angular Momentum* (Wiley, New York, 1957).
[22]C. L. French, C. E. Brion, A. O. Bawagan, P. S. Bagus, and E. R. Davidson, Chem. Phys. **121**, 315 (1988).
[23]A. W. Potts and T. A. Williams, J. Electron Spectrosc. Relat. Phenom. **3**, 3 (1974).
[24]S. Svensson, M. Carlsson-Göthe, L. Karlsson, A. Nilsson, N. Mårtensson, and U. Gelius, Phys. Scr. **44**, 184 (1991).
[25]M. Lebech, J. C. Houver, G. Raseev, A. S. dos Santos, D. Dowek, and R. R. Lucchese, J. Chem. Phys. **136**, 094303 (2012).
[26]M. Ehara, M. Ishida, and H. Nakatsuji, Collect. Czech. Chem. Commun. **70**, 881 (2005).
[27]P. Baltzer, M. Lundqvist, B. Wannberg, L. Karlsson, M. Larsson, M. A. Hayes, J. B. West, M. R. F. Siggel, A. C. Parr, and J. L. Dehmer, J. Phys. B: At., Mol. Opt. Phys. **27**, 4915 (1994).
[28]G. R. Wight, M. J. Van der Wiel, and C. E. Brion, J. Phys. B: At., Mol. Phys. **9**, 675 (1976).
[29]M. Lebech, J. C. Houver, and D. Dowek, J. Chem. Phys. **130**, 194307 (2009).
[30]Y. Hikosaka and J. H. D. Eland, Phys. Chem. Chem. Phys. **2**, 4663 (2000).
[31]Y. Hikosaka and J. H. D. Eland, Chem. Phys. **281**, 91 (2002).
[32]J. H. D. Eland and E. J. Duerr, Chem. Phys. **229**, 13 (1998).
[33]F. L. Yip, C. W. McCurdy, and T. N. Rescigno, Phys. Rev. A **90**, 063421 (2014).